

# AN ESTIMATE OF THE PRIMORDIAL NON-GAUSSIANITY PARAMETER $f_{NL}$ USING THE NEEDLET BISPECTRUM FROM WMAP

ØYSTEIN RUDJORD<sup>1,2</sup>, FRODE K. HANSEN<sup>2</sup>, XIAOHONG LAN<sup>3</sup>,  
MICHELE LIGUORI<sup>4</sup>, DOMENICO MARINUCCI<sup>3</sup>, SABINO MATARRESE<sup>5</sup>

*Draft version November 2, 2018*

## ABSTRACT

We use the full bispectrum of spherical needlets applied to the WMAP data of the cosmic microwave background as an estimator for the primordial non-Gaussianity parameter  $f_{NL}$ . We use needlet scales up to  $\ell_{\max} = 1000$  and the KQ75 galactic cut and find  $f_{NL} = 84 \pm 40$  corrected for point source bias. We also introduce a set of consistency tests to validate our results against the possible influence of foreground residuals or systematic errors. In particular, fluctuations in the value of  $f_{NL}$  obtained from different frequency channels, different masks and different multipoles are tested against simulated maps. All variations in  $f_{NL}$  estimates are found statistically consistent with simulations.

*Subject headings:* cosmic microwave background — cosmology: observations — methods: statistical

## 1. INTRODUCTION

The theory of inflation predicts the fluctuations in the Cosmic Microwave Background (CMB) to be close to Gaussian distributed. However, a small degree of non-Gaussianity is generally present in all the inflationary scenarios. The primordial non-Gaussian signal predicted by many models can be parametrized in the form:

$$\Phi(\mathbf{x}) = \Phi_L(\mathbf{x}) + f_{NL} (\Phi_L^2(\mathbf{x}) - \langle \Phi_L^2(\mathbf{x}) \rangle), \quad (1)$$

where  $\Phi(\mathbf{x})$  is the primordial curvature perturbation field at the end of inflation and  $\Phi_L(\mathbf{x})$  is the Gaussian part of the perturbation. The dimensionless parameter  $f_{NL}$  describes the amplitude of non-Gaussianity. The non-Gaussian part of the primordial curvature perturbation is a local functional of the Gaussian part and for this reason this kind of parametrization is often referred to as *local* non-Gaussianity. Local non-Gaussianity is predicted to arise from standard single-field slow-roll inflation (Acquaviva et al. 2003; Maldacena 2003) as well as from alternative inflationary scenarios for the generation of primordial perturbations, like the curvaton (Enqvist & Sloth 2002; Lyth & Wands 2002; Moroi & Takahashi 2001) or inhomogeneous (pre)reheating models (Dvali et al. 2004; Kolb et al. 2005, 2006), or even from alternatives to inflation, such as ekpyrotic and cyclic models (Koyama et al. 2007; Buchbinder et al. 2008). Other models, such as DBI inflation (Alishahiha et al. 2004) and ghost inflation (Arkani-Hamed et al. 2004), predict a different kind of primordial non-Gaussianity, called "equilateral", because the three point function for this kind of non-Gaussianity is peaked on equilateral configurations, in which the lengths of the three

wavevectors forming a triangle in Fourier space are equal (Creminelli et al. 2006). In this paper we will focus only on non-Gaussianity of the local type, described by equation 1. The interesting aspect of primordial non-Gaussianity is that the expected non-Gaussian amplitude  $f_{NL}$  varies significantly from model to model. Putting experimental bounds on  $f_{NL}$  is then equivalent to constraining primordial scenarios of inflation. For example standard single-field slow-roll inflation predicts  $f_{NL} \sim 10^{-2}$  at the end of inflation (Acquaviva et al. 2003; Maldacena 2003) (and therefore a final value  $\sim$  unity after general relativistic second-order perturbation effects are taken into account (Bartolo et al. 2004b,c)). Such a small value is not experimentally detectable and for this reason an eventual detection of a Gaussian signal in present and forthcoming CMB data will rule out single-field slow-roll inflation as a viable scenario. Motivated by these considerations many groups have attempted to measure  $f_{NL}$  using CMB datasets, and WMAP data in particular.

A detection of non-zero  $f_{NL}$  at more than the  $2\sigma$  level was found by (Yadav & Wandelt 2008) using the WMAP data with the Kp0 galactic cut. The WMAP team found similar values but stating that only the value obtained with the slightly larger KQ75 galactic cut is reliable due to possible foreground residuals. In this case a value of  $f_{NL} = 51 \pm 32$  was found. In both these cases, an extended version (Creminelli et al. 2006; Yadav & Wandelt 2008; Yadav et al. 2007b) of the (Komatsu et al. 2005) (KSW-method) based on the full bispectrum was used. Consistent results were found by (Curto et al. 2008) and (Pietrobon et al. 2008a) using parts of the bispectrum of spherical Mexican hat wavelets (Martinez-Gonzalez et al. 2002) and the skewness of needlet coefficients. A recent estimate has now been made by (Smith et al. 2008) obtaining the smallest error bars on  $f_{NL}$  so far finding  $f_{NL} = 38 \pm 21$ .

Recently, it was shown in (Lan & Marinucci 2008a) that needlet coefficients can be used to construct statistics which are directly related to the bispectrum. These statistics share most of the useful properties of the bispectrum, while at the same time they do present important advantages, especially in terms of robustness

<sup>1</sup> email: oystein.rudjord@astro.uio.no

<sup>2</sup> Institute of Theoretical Astrophysics, University of Oslo, P.O. Box 1029 Blindern, N-0315 Oslo, Norway

<sup>3</sup> Dipartimento di Matematica, Università di Roma 'Tor Vergata', Via della Ricerca Scientifica 1, I-00133 Roma, Italy

<sup>4</sup> Department of Applied Mathematics and Theoretical Physics, Centre for Mathematical Sciences, University of Cambridge, Wilberforce Road, Cambridge, CB3 0WA, United Kingdom

<sup>5</sup> Dipartimento di Fisica, G. Galilei, Università di Padova and INFN, Sezione di Padova, via Marzolo 8, I-35131 Padova, Italy

to masked data and computational rapidity. Motivated from these results, in this paper we will use the full bispectrum of needlet coefficients as an estimator of  $f_{NL}$ , introducing moreover a set of consistency tests to check the stability of our findings. In particular, we shall investigate whether changes in the estimated values of  $f_{NL}$  using different galactic cuts, different frequency bands and different multipoles are within the variations expected from simulations. Of course, variations in  $f_{NL}$  among these different cases which are significantly larger than statistical fluctuations might point out the presence of foreground residuals or other systematic effects that could have biased the estimate of  $f_{NL}$ .

The plan of the paper is as follows. In section 2, we describe the data used in the analysis. Then in section 3, the needlets and the needlet bispectrum estimator are described in detail. Finally, the results on the WMAP data are presented in section 4 and conclusions are made in section 5.

## 2. DATA

For this analysis we used the noise weighted average of the V and W frequency band of the WMAP 5 year CMB map, as well as the corresponding instrumental beam and noise properties. We have also performed the analysis on the individual Q (41 GHz), V (61 GHz) and W (94 GHz) bands. For masking out galactic foregrounds and point sources, we used the *KQ75* and *KQ85* mask supplied by the WMAP team. For particular cases, we also used the much smaller *Kp12* mask (maintaining 94% of the sky) as well as an extended *KQ75+* mask. The *KQ75+* mask is constructed from the *KQ75* mask, extending the mask with 5 degrees along the rim, maintaining a total of 63% of the sky. We have used the maps at Healpix<sup>6</sup> resolution  $N_{side} = 512$ .

## 3. METHOD

### 3.1. Spherical needlets

Needlets are a new form of (second generation) spherical wavelets, which were introduced into functional analysis by ((Narcowich et al. 2006a,b)) and have attracted a lot of attention in the cosmological literature hereafter. The possibility to use needlets for the statistical analysis of spherical random fields, with a view to CMB applications, is first discussed in (Baldi et al. 2006), where the stochastic properties of needlet coefficients are established and their possible roles for data analysis (spectrum estimation, Gaussianity testing) are described; further mathematical properties were then given in (Baldi et al. 2007). The first application to CMB data, in particular, for the analysis of cross-correlation of CMB and Large Scale Structure data was provided by (Pietrobon et al. 2006); a general presentation of the method for a CMB audience is given in (Marinucci et al. 2008), while in (Guiloux et al. 2007) the properties of different weighting schemes are investigated and compared. Further papers have applied needlets on CMB data, for issues such as map-making, spectrum estimation, detection of features and anisotropies ((Fay et al. 2008b; Delabrouille et al. 2008; Fay et al. 2008a; Pietrobon et al. 2008b)); more

recently, needlets have also been considered for the analysis of directional data, with a view to high energy cosmic rays ((Baldi et al. 2008)) and for the analysis of polarization data ((Geller & Marinucci 2008; Geller et al. 2008)), whereas extensions to the so-called Mexican needlets case are discussed by (Geller & Mayeli 2007b,a), their stochastic properties being established in (Lan & Marinucci 2008b; Mayeli 2008).

The spherical needlet (function) is defined as

$$\psi_{jk}(\hat{\gamma}) = \sqrt{\lambda_{jk}} \sum_{\ell} b\left(\frac{\ell}{B^j}\right) \sum_{m=-\ell}^{\ell} \bar{Y}_{\ell m}(\hat{\gamma}) Y_{\ell m}(\gamma_k); \quad (2)$$

here,  $\hat{\gamma}$  is a direction on the sphere, and  $j$  is the frequency (multipole range) of the needlet and  $\lambda_{jk}$  is a normalizing factor. The points  $\{\gamma_k\}$  can be identified with the pixel centres in the HealPix pixelization scheme. The number  $B$  defines the needlet basis such that only multipoles in the range  $\ell = [B^{j-1}, B^{j+1}]$  are included, i.e. the function  $b(\ell/B^j)$  is zero outside this range. For details in the functional form of  $b(\ell/B^j)$ , please refer to (Marinucci et al. 2008) and references therein.

The advantages of needlets have already been discussed in several papers in the literature; in short, we recall that needlets do not rely on any tangent plane approximation; they are computationally very convenient, and inherently adapted to standard packages such as HealPix; they allow for a simple reconstruction formula (a property which is *not* shared by other wavelets systems); they are quasi-exponentially (i.e. faster than any polynomial) concentrated in pixel space. Moreover, needlets are exactly localized on a finite number of multipoles (the width of this support is explicitly known and can be specified as an input parameter, see Eq. 2)).

Random needlet coefficients can be shown to be asymptotically uncorrelated (and hence, in the Gaussian case, independent) at any fixed angular distance, when the frequency increases. This capital property is in general not shared by other wavelet systems (see ((Lan & Marinucci 2008b; Mayeli 2008))) and can be exploited in several statistical procedures, as it allows one to treat needlet coefficients as a sample of independent and identically distributed coefficients on small scales, at least under the Gaussianity assumption.

In this paper, for notational simplicity we shall take random needlet coefficients to be

$$\beta_{jk} = \sum_{\ell} b\left(\frac{\ell}{B^j}\right) \sum_{m=-\ell}^{\ell} a_{\ell m} Y_{\ell m}(\hat{\gamma}_k) \equiv \sum_{\ell m} b_{\ell} a_{\ell m} Y_{\ell m}(\hat{\gamma}_k)$$

Here  $j$  denotes the frequency of the coefficient and  $\hat{\gamma}_k$  denotes the direction on the sky. We are dropping a normalizing term  $\sqrt{\lambda_{jk}}$ ; this comes at no cost, because in this paper needlet coefficients always appear after normalization with their own standard deviation, so that this deterministic factor cancels. From the notational point of view, however, this allows a major simplification, as it permits to avoid considering different weights at different frequencies  $j$ . As before, the index  $k$  can in practice be the pixel number on the HEALPix grid.

### 3.2. The needlets bispectrum

<sup>6</sup> <http://healpix.jpl.nasa.gov>

Starting from some highly influential papers ((Hu et al. 2001; Komatsu & Spergel 2001)), the bispectrum has emerged in the last decade as the most promising statistics for the detection of non-Gaussianity in CMB data. To fix notation, we recall that, under the assumption of statistical isotropy for CMB radiation, we must have ((Hu et al. 2001))

$$\langle a_{\ell_1 m_1} a_{\ell_2 m_2} a_{\ell_3 m_3} \rangle = \begin{pmatrix} \ell_1 & \ell_2 & \ell_3 \\ m_1 & m_2 & m_3 \end{pmatrix} B_{\ell_1 \ell_2 \ell_3},$$

where on the right hand side we have introduced the Wigner's 3j coefficients, which are different from zero only for configurations of  $l_1, l_2, l_3$  which satisfy the triangle conditions (see again (Hu et al. 2001; Komatsu & Spergel 2001)). The *unreduced bispectrum*  $B_{\ell_1 \ell_2 \ell_3}$  is identically zero in the Gaussian case; under non-Gaussianity, it can be estimated by

$$\widehat{B}_{\ell_1 \ell_2 \ell_3} = \sum_{m_1 m_2 m_3} \begin{pmatrix} \ell_1 & \ell_2 & \ell_3 \\ m_1 & m_2 & m_3 \end{pmatrix} a_{\ell_1 m_1} a_{\ell_2 m_2} a_{\ell_3 m_3}.$$

It was shown by ((Komatsu & Spergel 2001)) that, in the idealistic circumstance with the absence of masked regions, the bispectrum can constrain non-Gaussianity very efficiently, with a signal-to-noise ratio equal to unity for  $f_{NL}$  smaller than 10 at the Planck resolution. In the presence of masked regions, however, these properties deteriorate consistently; many statistical solutions have been discussed so far, see for instance (Yadav et al. 2007; Yadav & Wandelt 2008) for the most recent developments. A large literature has also focused on the determinations of the multipole configurations where the signal-to-noise ratio should be expected to be stronger, in view of a given model: see for instance (Babich et al. 2004; Cabella et al. 2006; Bartolo et al. 2004a; Marinucci 2006; Yadav & Wandelt 2008) and many others.

Our purpose in this paper is to combine ideas from the bispectrum and the needlets literature, to propose a needlet bispectrum method to test non-Gaussianity and estimate the nonlinearity parameter  $f_{NL}$ . More precisely, we suggest to focus on the needlet bispectrum, defined by

$$I_{j_1 j_2 j_3} = \sum_k \frac{\beta_{j_1 k} \beta_{j_2 k} \beta_{j_3 k}}{\sigma_{j_1 k} \sigma_{j_2 k} \sigma_{j_3 k}},$$

where  $\sigma_j = \sqrt{\langle \beta_{jk}^2 \rangle}$  is the standard deviation of  $\beta_{jk}$ . The needlet bispectrum was first considered in ((Lan & Marinucci 2008a)), and we refer to that paper for more discussion and details on its mathematical properties; the use of needlets for a non-Gaussianity test is also proposed in (Pietrobon et al. 2008a), where the focus is instead on the skewness of the coefficients (which can be viewed as a special case of the bispectrum, for  $j_1 = j_2 = j_3$ ). Of course, many other papers had previously used wavelet-related techniques to search for non-Gaussianity in CMB, see for instance (Vielva et al. 2004; Cruz et al. 2007, 2006; McEwen et al. 2006).

In short, to understand the motivations of our proposals, note that, denoting by  $N$  the cardinality of the points  $k$  (i.e., the number of points in the pixelization scheme, so that  $4\pi/N$  provides an approximation for the

pixel area), and neglecting for simplicity beam factors, we have approximately

$$\begin{aligned} & \frac{4\pi}{N} \sum_k \beta_{j_1 k} \beta_{j_2 k} \beta_{j_3 k} = \\ & = \sum_{\ell_1 m_1} \sum_{\ell_2 m_2} \sum_{\ell_3 m_3} b\left(\frac{\ell_1}{B^{j_1}}\right) b\left(\frac{\ell_2}{B^{j_2}}\right) b\left(\frac{\ell_3}{B^{j_3}}\right) \\ & \times \frac{4\pi}{N} \sum_k a_{\ell_1 m_1} a_{\ell_2 m_2} a_{\ell_3 m_3} Y_{\ell_1 m_1}(\widehat{\gamma}_k) Y_{\ell_2 m_2}(\widehat{\gamma}_k) Y_{\ell_3 m_3}(\widehat{\gamma}_k) \\ & \simeq \sum_{\ell_i m_i} b\left(\frac{\ell_1}{B^{j_1}}\right) b\left(\frac{\ell_2}{B^{j_2}}\right) b\left(\frac{\ell_3}{B^{j_3}}\right) a_{\ell_1 m_1} a_{\ell_2 m_2} a_{\ell_3 m_3} \\ & \times \int Y_{\ell_1 m_1}(\widehat{\gamma}) Y_{\ell_2 m_2}(\widehat{\gamma}) Y_{\ell_3 m_3}(\widehat{\gamma}) d\widehat{\gamma}. \end{aligned}$$

Write

$$h_{\ell_1 \ell_2 \ell_3} = \begin{pmatrix} \ell_1 & \ell_2 & \ell_3 \\ 0 & 0 & 0 \end{pmatrix} \sqrt{\frac{(2\ell_1 + 1)(2\ell_2 + 1)(2\ell_3 + 1)}{4\pi}};$$

hence we obtain

$$\begin{aligned} & \sum_{\ell_i m_i} b\left(\frac{\ell_1}{B^{j_1}}\right) b\left(\frac{\ell_2}{B^{j_2}}\right) b\left(\frac{\ell_3}{B^{j_3}}\right) \\ & \times a_{\ell_1 m_1} a_{\ell_2 m_2} a_{\ell_3 m_3} \begin{pmatrix} \ell_1 & \ell_2 & \ell_3 \\ m_1 & m_2 & m_3 \end{pmatrix} h_{\ell_1 \ell_2 \ell_3} \\ & = \sum_{\ell_1 \ell_2 \ell_3} b\left(\frac{\ell_1}{B^{j_1}}\right) b\left(\frac{\ell_2}{B^{j_2}}\right) b\left(\frac{\ell_3}{B^{j_3}}\right) h_{\ell_1 \ell_2 \ell_3} \widehat{B}_{\ell_1 \ell_2 \ell_3}. \end{aligned}$$

From the previous computations, it should be clear that the needlets bispectrum can be viewed as a smoothed and normalized form of the standard bispectrum estimator. As usual with wavelet techniques, the advantage is that, while the standard bispectrum is known to be heavily affected by the presence of masked regions, needlet coefficients are much more robust and consequently the needlet bispectrum makes up a more reliable statistics even for incomplete maps. Furthermore, the needlet bispectrum is computationally very convenient, as it does not require the evaluation of Wigner's 3j coefficients, which is extremely time-consuming.

From the mathematical point of view, further properties of the needlets bispectrum are discussed by (Lan & Marinucci 2008a); in particular, it is shown that, after normalization,  $\widehat{I}_{j_1 j_2 j_3}$  is asymptotically Gaussian as the frequency increases. Furthermore, it can be shown that (under idealistic experimental circumstances) the values of the needlet bispectrum are asymptotically independent over different frequencies, so that chi-square statistics can be suitably implemented. In (Lan & Marinucci 2008a), some analytic discussion on the power properties of the needlet bispectrum for a pure Sachs-Wolfe model were also provided, showing that its expected value diverges to infinity at high frequencies. Although those results were derived in a mathematical

setting and did not take into account many features of CMB data, the simulations in the present paper show (in a much more realistic setting) that this procedure does have very satisfactory power properties in the presence of non-Gaussianity.

### 3.3. $f_{NL}$ estimator

We will now use the needlets bispectrum for estimating  $f_{NL}$  by a  $\chi^2$  minimization procedure. We define  $\chi^2(f_{NL})$  as

$$\chi^2(f_{NL}) = \mathbf{d}^T(f_{NL})\mathbf{C}^{-1}\mathbf{d}(f_{NL}),$$

where the elements  $d_i$  of the data vector  $\mathbf{d}$  are defined as  $d_i = I_{j_1 j_2 j_3}(\text{observed}) - \langle I_{j_1 j_2 j_3} \rangle(f_{NL})$  for all combinations of  $(j_1, j_2, j_3)$  satisfying the triangle condition. Here  $I_{j_1 j_2 j_3}(\text{observed})$  is the needlets bispectrum of the observed data and  $\langle I_{j_1 j_2 j_3} \rangle(f_{NL})$  is the expectation value of the needlet bispectrum for a given value of  $f_{NL}$ . The correlation matrix  $\mathbf{C}$  is given by

$$C_{ij} = \langle d_i d_j \rangle - \langle d_i \rangle \langle d_j \rangle.$$

The correlation matrix is obtained from Gaussian simulations. In order to avoid cumbersome numeric grid-calculations of  $\langle I_{j_1 j_2 j_3} \rangle(f_{NL})$ , we seek an expression with a more explicit dependency of  $f_{NL}$ . In order to arrive at such an expression, we write out again the needlets bispectrum as

$$\begin{aligned} I_{j_1 j_2 j_3} &= \sum_k^{nix} \frac{\beta_{j_1 k} \beta_{j_2 k} \beta_{j_3 k}}{\sigma_{j_1 k} \sigma_{j_2 k} \sigma_{j_3 k}} \\ &= \sum_k \sum_{\ell_1 \ell_2 \ell_3} \sum_{m_1 m_2 m_3} \frac{b_{\ell_1}}{\sigma_{j_1 k}} \frac{b_{\ell_2}}{\sigma_{j_2 k}} \frac{b_{\ell_3}}{\sigma_{j_3 k}} a_{\ell_1 m_1} a_{\ell_2 m_2} a_{\ell_3 m_3} \\ &\times Y_{\ell_1 m_1}(\hat{\gamma}_k) Y_{\ell_2 m_2}(\hat{\gamma}_k) Y_{\ell_3 m_3}(\hat{\gamma}_k) \end{aligned} \quad (3)$$

As usual, the non-Gaussian  $a_{\ell m}$ 's are assumed to be a combination of a linear (Gaussian) and a non-linear term:  $a_{\ell m} = a_{\ell m}^G + f_{NL} a_{\ell m}^{NG}$ . This allows us to write the three-point correlations in  $a_{\ell m}$ 's as

$$\begin{aligned} &\langle a_{\ell_1 m_1} a_{\ell_2 m_2} a_{\ell_3 m_3} \rangle \\ &= \langle a_{\ell_1 m_1}^G a_{\ell_2 m_2}^G a_{\ell_3 m_3}^G \rangle + f_{NL} \langle \langle a_{\ell_1 m_1}^{NG} a_{\ell_2 m_2}^G a_{\ell_3 m_3}^G \rangle \rangle \\ &+ \langle \langle a_{\ell_1 m_1}^G a_{\ell_2 m_2}^{NG} a_{\ell_3 m_3}^G \rangle \rangle + \langle \langle a_{\ell_1 m_1}^G a_{\ell_2 m_2}^G a_{\ell_3 m_3}^{NG} \rangle \rangle \\ &+ \mathcal{O}((a_{\ell m}^{NG})^2) \end{aligned} \quad (4)$$

The non-linear terms are assumed to be small, and thus we will neglect the higher order terms,  $\mathcal{O}((a_{\ell m}^{NG})^2) \approx 0$ . We will also neglect the pure Gaussian term, since the three point correlation function of a Gaussian field is zero. We insert the remaining terms into eq. 3 and find

the mean value:

$$\begin{aligned} \langle I_{j_1 j_2 j_3} \rangle(f_{NL}) &= f_{NL} \left( \left\langle \sum_k^{nix} \frac{\beta_{j_1 k}^{NG} \beta_{j_2 k}^G \beta_{j_3 k}^G}{\sigma_{j_1 k} \sigma_{j_2 k} \sigma_{j_3 k}} \right\rangle \right) \\ &+ \left\langle \sum_k^{nix} \frac{\beta_{j_1 k}^G \beta_{j_2 k}^{NG} \beta_{j_3 k}^G}{\sigma_{j_1 k} \sigma_{j_2 k} \sigma_{j_3 k}} \right\rangle \\ &+ \left\langle \sum_k^{nix} \frac{\beta_{j_1 k}^G \beta_{j_2 k}^G \beta_{j_3 k}^{NG}}{\sigma_{j_1 k} \sigma_{j_2 k} \sigma_{j_3 k}} \right\rangle \\ &\approx f_{NL} \left( \langle I_{j_1 j_2 j_3}^{NG, G, G} \rangle + \langle I_{j_1 j_2 j_3}^{G, NG, G} \rangle + \langle I_{j_1 j_2 j_3}^{G, G, NG} \rangle \right) \\ &= f_{NL} \langle \hat{I}_{j_1 j_2 j_3} \rangle \end{aligned} \quad (5)$$

where we have defined the quantity

$$\langle \hat{I}_{j_1 j_2 j_3} \rangle = \langle I_{j_1 j_2 j_3}^{NG, G, G} \rangle + \langle I_{j_1 j_2 j_3}^{G, NG, G} \rangle + \langle I_{j_1 j_2 j_3}^{G, G, NG} \rangle$$

which does not depend on  $f_{NL}$  to the first order in  $a_{\ell m}^{NG}$ . Figure 1 shows a plot of a average needlet bispectrum  $\langle I_{j_1 j_2 j_3} \rangle(f_{NL})$  from 300 simulations with  $f_{NL} = 500$ . Here the bispectrum is plotted along one of the indices  $j_1 = j$ , while the two other indices  $j_2 = 25$  and  $j_3 = 25$  are kept constant. In the same plot is also our first order approximation,  $500 \times \langle \hat{I}_{j_1 j_2 j_3} \rangle$ . As we see, this approximation is fairly good for  $f_{NL} = 500$ , and based on previous estimates ((Komatsu et al. 2008)), we will assume that  $f_{NL}$  does not have a value significantly higher than this.

We can now write the elements of the data vector  $\mathbf{d}$  of the  $\chi^2$  as  $d_i = I_{j_1 j_2 j_3} - f_{NL} \langle \hat{I}_{j_1 j_2 j_3} \rangle$ . In order to estimate  $f_{NL}$ , we need to find the value of  $f_{NL}$  that minimizes the  $\chi^2$

$$\frac{d\chi^2(f_{NL})}{df_{NL}} = 0. \quad (6)$$

giving

$$f_{NL} = \frac{\langle \hat{I}_{j_1 j_2 j_3} \rangle^T \mathbf{C}^{-1} I_{j_1 j_2 j_3}(\text{observed})}{\langle \hat{I}_{j_1 j_2 j_3} \rangle^T \mathbf{C}^{-1} \langle \hat{I}_{j_1 j_2 j_3} \rangle}. \quad (7)$$

### 3.4. The procedure to estimate $f_{NL}$

We will now show the full procedure we have used to estimate  $f_{NL}$  using the needlet bispectrum.

1. Generate 10000 simulations of Gaussian sky maps using the best fit WMAP 5 year power spectrum. These are smoothed with an instrumental beam and noise is added. The maps are also multiplied with a mask for galactic cut, in order to remove foregrounds. A needlet transform is applied and the standard deviation  $\sigma_{jk}$  of the needlet coefficients  $\beta_{jk}$  are found. This standard deviation is needed to find the needlet bispectrum as seen from eq. (3).
2. Produce another 120000 Gaussian simulations. Mask, beam and noise properties are applied as above. The needlet coefficients are found and used

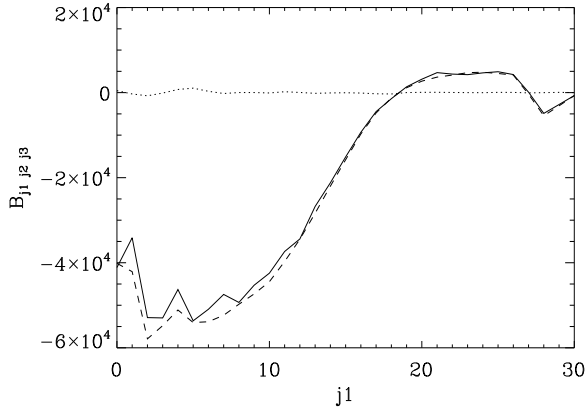


FIG. 1.—  $\hat{I}_{j_1 j_2 j_3}$  (dashed) plotted along  $j_1 = j$  while  $j_2 = 25$  and  $j_3 = 25$ , compared to the average bispectrum from 300 simulations with  $f_{NL} = 500$  (full line) and average bispectrum from 10000 Gaussian simulations (dotted).

to obtain the needlet bispectra,  $I_{j_1 j_2 j_3}$ . These bispectra are used to find the covariance matrix  $\mathbf{C}$ . This converges very slowly, thus the need for such a large number of simulations.

3. Generate 300 non-Gaussian simulations ((Liguori et al. 2007)) to find the mean first order non-Gaussian bispectrum,  $\langle \hat{I}_{j_1 j_2 j_3} \rangle$ .
4. Obtain the needlet bispectrum from the data and estimate  $f_{NL}$  using eq. 7
5. Generate a set of 10000 simulated Gaussian maps and estimate  $f_{NL}$  in the same manner from these maps in order to obtain the error bars on  $f_{NL}$ . This set of estimated  $f_{NL}$  values form a Gaussian distribution around  $f_{NL} = 0$ . Figure 2 shows a histogram of the 10000  $f_{NL}$  of the V+W frequency channel estimates plotted together with a Gaussian distribution. We see that the distribution of  $f_{NL}$  estimates is very close to Gaussian, so we will use the standard deviation as a measure of the uncertainty of the estimate.

#### 4. RESULTS

##### 4.1. Estimates of $f_{NL}$

We used the above procedure to estimate  $f_{NL}$  from the WMAP data. The co-added V+W map as well as the single frequency bands Q, V and W were used. The estimated values of  $f_{NL}$  are listed in table 1 together with the  $1\sigma$  error bars found from the simulations. For the analysis we used both the *KQ85* mask and the more aggressive *KQ75* mask for galactic cut in order to study potential effects from residual foregrounds.

We have used multipoles up to  $\ell_{max} = 1024$  in the analysis. We tested different values of  $B$  in order to find the number of needlet scales from  $\ell = 2$  to  $\ell = 1000$  which would yield an invertible covariance matrix. We found that the maximum number of scales which could be used was 31 scales, using  $B = 1.2050$ . For comparison with the WMAP results we also used needlet scales including multipoles up to  $\ell_{max} = 500$  and  $\ell_{max} = 700$ . In table 1 as well as in the following text, we will use  $\ell_{max} =$

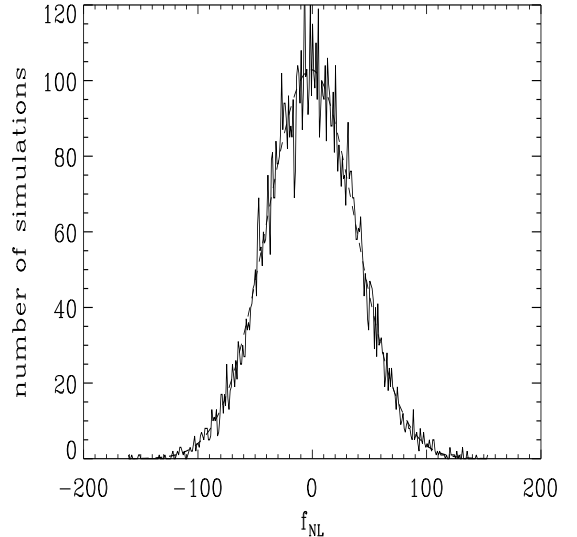


FIG. 2.— A histogram (full line) of  $f_{NL}$  estimates of 10000 Gaussian simulations of the V+W channel plotted together with a Gaussian fit (dashed). As expected the  $f_{NL}$  values form an approximate Gaussian distribution with a mean value of  $f_{NL} = 0$ .

1000, 700, 500 to specify the highest multipole included in the highest needlet scale. Note that this number may differ slightly from 1000, 700 and 500 depending on the exact value of  $B$  specified. For  $\ell_{max} = 500$ , we used 30 scales with  $B = 1.1828$  and for  $\ell_{max} = 700$  we used 31 scales with  $B = 1.1880$ .

We see from the table that the best results obtained on the combined V+W band yields  $f_{NL} = 89 \pm 39$  for the *KQ75* cut and  $f_{NL} = 117 \pm 36$  using the smaller *KQ85* cut. We run simulations of unresolved point sources based on the procedure described in (Komatsu et al. 2008) and obtained a point source bias of  $\Delta f_{NL} = 5 \pm 1$  for *KQ75* and  $\Delta f_{NL} = 7 \pm 1$  for *KQ85* giving corrected values of  $f_{NL} = 84 \pm 40$  and  $f_{NL} = 110 \pm 37$ . We see that even for *KQ75* a zero value for  $f_{NL}$  is excluded at about  $2\sigma$ . In order to make sure that foregrounds are not influencing our results significantly, we also make an estimate on the much larger *KQ75+* mask and obtain  $f_{NL} = 103 \pm 41$  or  $f_{NL} = 97 \pm 42$  taking into account unresolved point sources.

As we see there is a large improvement in error bars from  $\ell_{max} = 700$  to  $\ell_{max} = 1000$ . This may seem at first sight surprising taking into account the fact that this range is noise dominated. However, this result is not unexpected if we take into account the way the needlets are constructed. Indeed,  $\ell_{max} = 700$  means that no needlet scale using information above  $\ell_{max} = 700$  is included. Nevertheless, from the previous description of the needlet systems it is easy to see that the information from multipoles close to the boundary value  $\ell_{max} = 700$  will receive very little weight in general. Of course, the next needlet scale will contain information below as well as above  $\ell_{max} = 700$ . Therefore, when extending the analysis to higher  $\ell$ 's we do not only exploit 300 more multipoles, but we are also able to extract better information from the multipoles below  $\ell = 700$ .

Another test was performed to take advantage of the

freq. channel	mask	$\ell_{max}$	$n_j$	$f_{NL}$
V+W	<i>KQ85</i>	700	31	$156 \pm 45$
V+W	<i>KQ75</i>	700	32	$88 \pm 48$
V+W	<i>Kp12</i>	1000	31	$160 \pm 30$
V+W	<i>KQ85</i>	1000	31	$117 \pm 36$
V+W	<i>KQ75</i>	1000	31	$89 \pm 39$
V+W	<i>KQ75+</i>	1000	31	$103 \pm 41$
V+W (Raw)	<i>KQ85</i>	1000	31	$105 \pm 36$
V+W (Raw)	<i>KQ75</i>	1000	31	$83 \pm 39$
V+W (Raw)	<i>KQ75+</i>	1000	31	$87 \pm 41$
V	<i>KQ75</i>	500	30	$78 \pm 57$
V	<i>KQ85</i>	1000	31	$100 \pm 39$
V	<i>KQ75</i>	1000	31	$105 \pm 42$
V (Raw)	<i>KQ85</i>	1000	31	$88 \pm 39$
V (Raw)	<i>KQ75</i>	1000	31	$100 \pm 42$
W	<i>KQ75</i>	500	30	$57 \pm 59$
W	<i>KQ85</i>	1000	31	$79 \pm 42$
W	<i>KQ75</i>	1000	31	$54 \pm 45$
W (Raw)	<i>KQ85</i>	1000	31	$57 \pm 42$
W (Raw)	<i>KQ75</i>	1000	31	$41 \pm 45$
Q	<i>KQ75</i>	500	30	$47 \pm 59$
Q	<i>KQ85</i>	1000	31	$33 \pm 42$
Q	<i>KQ75</i>	1000	31	$9 \pm 44$
Q (Raw)	<i>KQ85</i>	1000	31	$-64 \pm 42$
Q (Raw)	<i>KQ75</i>	1000	31	$-21 \pm 44$
Combined V and W	<i>KQ75</i>	1000	30	$76 \pm 38$

TABLE 1

THE ESTIMATED VALUES FOR  $f_{NL}$  TOGETHER WITH THE  $1\sigma$  ERROR BARS.

fact that the CMB should be independent of frequency, while the noise differs between the channels. A data vector was composed from the needlet bispectrum of both the individual V and W frequency channels.

$$\mathbf{d} = \begin{bmatrix} I_{j_1 j_2 j_3}^V \\ \vdots \\ I_{j_1 j_2 j_3}^W \\ \vdots \end{bmatrix} \quad (8)$$

The full covariance matrix in this case contains information about correlations between the frequencies, and should therefore enable us to get smaller error-bars on  $f_{NL}$ . However, for this analysis it was necessary to use only 30 needlet scales from each frequency channel in order to get an invertible covariance matrix. And the result (shown in the bottom row of table 1) was not a large improvement from the analysis of the VW band at 31 needlet scales. However this is our estimate for  $f_{NL}$  with the smallest error-bars while using the *KQ75* mask.

For the  $B = 1.2050$  case for the V+W band with the *KQ75* mask, we have also investigated the change in  $f_{NL}$  as a function of the number of needlet scales included. We thus included only the first 25 needlet scales (up to  $\ell_{max} = 324$ ), then the 26 first scales (up to  $\ell_{max} = 390$ ) and so on up to all 31 scales. The results are presented in table 2. As expected, we see that the error bars are decreasing with increasing  $\ell_{max}$ . Differently from our case, in the optimal bispectrum estimation performed by the WMAP team and other groups error bars saturates earlier than  $\ell_{max} = 1000$  because the full inverse covariance weighting scheme is not implemented and an approximation is used (whereas in this case the Monte Carlo approach used to estimate the bispectrum automatically

accounts for this issue). Note however the WMAP error bars at  $\ell_{max} = 700$  are still smaller than ours at  $\ell_{max} = 1000$  because we don't implement a minimum variance estimator and thus we don't saturate the Rao-Cramer bound. Moreover an optimal bispectrum estimator with full inverse covariance weighting has been very recently implemented by Smith et al. 2008.

$\ell_{max}$	$n_j$	V+W	V	W	Q
324	25	$64 (\pm 71)$	$77 (\pm 73)$	$63 (\pm 75)$	$26 (\pm 74)$
390	26	$44 (\pm 61)$	$81 (\pm 64)$	$35 (\pm 66)$	$25 (\pm 66)$
471	27	$44 (\pm 55)$	$71 (\pm 60)$	$40 (\pm 62)$	$31 (\pm 62)$
567	28	$42 (\pm 52)$	$56 (\pm 56)$	$55 (\pm 58)$	$43 (\pm 56)$
683	29	$73 (\pm 49)$	$71 (\pm 52)$	$72 (\pm 54)$	$23 (\pm 50)$
823	30	$81 (\pm 43)$	$80 (\pm 46)$	$72 (\pm 49)$	$24 (\pm 46)$
1000	31	$89 (\pm 39)$	$105 (\pm 42)$	$54 (\pm 45)$	$9 (\pm 44)$

TABLE 2

THE ESTIMATED VALUES FOR  $f_{NL}$  FOR DIFFERENT NUMBER  $n_j$  OF NEEDLET SCALES. SINCE ERROR BARS INCREASE WHEN USING FEW NEEDLET SCALES, THE CORRESPONDING  $1\sigma$  ERROR ESTIMATE IS GIVEN IN PARENTHESIS.

#### 4.2. Consistency checks

We see from these results that the estimates using the *KQ85* mask differs notably from the estimates using the *KQ75* mask. This is particularly the case for the V+W channel, when only considering scales up to  $\ell_{max} = 700$ . This estimate when using the *KQ85* mask ( $f_{NL} = 156$ ) is much higher than the estimate found from the same map, using the *KQ75* mask ( $f_{NL} = 88$ ). We are therefore motivated to study simulations to find how often a change of mask triggers such a large difference in the estimate.

We consider two sets of 10000 CMB sky simulations, each set generated using the same random seed, and therefore identical. One set is multiplied with the *KQ75* mask, while the other is multiplied with the *KQ85* mask. Now we estimate  $f_{NL}$  for both sets, and find the difference between each estimate, and the corresponding estimate from the identical map with the other mask,  $\Delta f_{NL} = f_{NL}^{KQ75} - f_{NL}^{KQ85}$ . Then the mean value and standard deviation of  $\Delta f_{NL}$  is found.

For  $\ell_{max} = 1000$  we found  $\Delta f_{NL} = 28$  for the WMAP data, whereas the standard deviation  $\sigma_{\Delta f_{NL}} = 21$  for simulations. For  $\ell_{max} = 700$ , we found  $\Delta f_{NL} = 68$  and  $\sigma_{\Delta f_{NL}} = 34$ . In the first case, the shift in  $f_{NL}$  when changing mask is as expected whereas in the latter case, the change  $\Delta f_{NL}$  is slightly high, but only at the  $2\sigma$  level.

As a further test of consistency, we also considered the difference in  $f_{NL}$  estimate between  $\ell_{max} = 700$  and  $\ell_{max} = 1000$  when using the *KQ85* galactic cut  $\Delta f_{NL} = f_{NL}^{\ell_{max}=700} - f_{NL}^{\ell_{max}=1000} = 39$ . However, a comparison with simulations reveal that  $\Delta f_{NL}$  have a standard deviation of  $\sigma = 30$ . In other words, the difference in the two estimates is well within  $2\sigma$  and is to be expected.

To test the variation of  $f_{NL}$  with increasing galactic cut, we estimated  $f_{NL}$  using the tiny *Kp12* mask as well as the extended *KQ75+* mask. We see that  $f_{NL}$  decrease when going from the smallest mask to *KQ85* and *KQ75*, but increases slightly again to *KQ75+*.

At this point a  $\chi^2$  test was implemented. Three identical sets of 10000 simulations were generated, and each set was multiplied with one of the KQ85, KQ75 and KQ75+ masks (we do not include the Kp12 mask as foregrounds are likely to be important for such a small mask). For each simulation, a data vector,  $\mathbf{d}$ , with two elements was formed from the difference in  $f_{NL}$  estimates between three different masks:

$$\mathbf{d} = \begin{bmatrix} f_{NL}^{KQ75} - f_{NL}^{KQ85} \\ f_{NL}^{KQ75+} - f_{NL}^{KQ75} \end{bmatrix} \quad (9)$$

Of the 10000 simulations, 5000 were used to find a mean value and covariance matrix for  $\mathbf{d}$ . Then a  $\chi^2$  value was found for each of the remaining 5000 simulations as follows:

$$\chi^2 = (\mathbf{d} - \langle \mathbf{d} \rangle)^T C^{-1} (\mathbf{d} - \langle \mathbf{d} \rangle) \quad (10)$$

A similar  $\chi^2$  value was found from the  $f_{NL}$  values of the WMAP data maps. Then the  $\chi^2$  values for the simulations were compared with that of the WMAP data.

The result was that 37% of the simulations had a higher value of  $\chi^2$ . We conclude that the variation of the  $f_{NL}$  estimate for different masks (larger than Kp12) are within expectations for a Gaussian map.

As a further check for possible foreground contamination we will check the variation of  $f_{NL}$  with frequency channel. We investigated this by estimating  $f_{NL}$  using 10000 simulated Gaussian CMB sky maps. For each simulated sky, three identical maps were generated. These maps were then smoothed with the instrumental beam of the Q, V and W frequency channel respectively, and noise was added independently to each of the maps. For each of these sets of simulations a needlet transform was performed using 31 needlet scales in the range  $2 \leq \ell \leq 1000$ . Then the bispectra were found and  $f_{NL}$  was estimated, using between 25 and 31 of the needlet scales.

At this point we performed a  $\chi^2$  test, similar to the one described above. First we tested the variation between the frequency channels when using all 31 of the needlet scales. For every simulation, a data vector,  $\mathbf{d}$ , with two elements was formed from the difference in  $f_{NL}$  estimates between the channels.

$$\mathbf{d} = \begin{bmatrix} f_{NL}^Q - f_{NL}^V \\ f_{NL}^V - f_{NL}^W \end{bmatrix} \quad (11)$$

The results using the KQ75 mask showed that only 4.5% of the simulations had a higher  $\chi^2$  value, than the WMAP data. This corresponds to a  $\approx 2\sigma$  deviation.

To investigate whether this is consistent on several scales, we also performed the same test with some of the needlet scales removed. This was done using between 25 and 31 needlet scales. Finally we combined the data vectors from all these tests:

$$\mathbf{d} = \begin{bmatrix} f_{NL}^{Q31} - f_{NL}^{V31} \\ f_{NL}^{V31} - f_{NL}^{W31} \\ f_{NL}^{Q30} - f_{NL}^{V30} \\ f_{NL}^{V30} - f_{NL}^{W30} \\ \vdots \\ f_{NL}^{Q25} - f_{NL}^{V25} \\ f_{NL}^{V25} - f_{NL}^{W25} \end{bmatrix} \quad (12)$$

and used this to make a combined test. From the KQ75 results (shown in table 3) it seems that only by using all available scales we find a small inconsistency of the  $f_{NL}$  values between frequency channels. We repeated the latter test using the smaller KQ85 cut and found in this case that 14% of the simulations had a higher  $\chi^2$  concluding that foreground residuals do not appear to be causing the difference in  $f_{NL}$  for different channels.

$\ell_{max}$	needlet scales	% of sim. with higher $\chi^2$
324	25	20.6
390	26	21.3
471	27	54.6
567	28	95.0
683	29	43.2
823	30	33.4
992	31	4.5
all of the above		12.2

TABLE 3  
TEST OF DIFFERENCE BETWEEN FREQUENCY CHANNELS USING DIFFERENT NUMBER OF SCALES. THE LAST ROW COMBINES ALL THE OTHER VARIABLES IN ONE TEST. THE TABLE SHOWS PERCENTAGE OF SIMULATIONS WITH HIGHER  $\chi^2$  THAN THE WMAP DATA USING THE KQ75 MASK.

To test the influence of foregrounds on the estimate of  $f_{NL}$ , we have estimated  $f_{NL}$  on the WMAP maps before foreground subtraction (raw maps). The results are listed in table 1. We see in particular for the Q band that the the value of  $f_{NL}$  is negatively biased by the presence of foregrounds. A similar result was also found in (Yadav & Wandelt 2008; Komatsu et al. 2008). Foreground residuals would thus be expected to give a too low value of  $f_{NL}$ . To check the power of our consistency test, we repeated the above  $\chi^2$  test of the differences in estimated  $f_{NL}$  between frequency channels using 31 scales. We find that only 0.7% of the simulations have a higher  $\chi^2$  than for the WMAP data for the KQ75 cut, and none of the simulations have a similarly high  $\chi^2$  for the KQ85 cut. The test thus shows a clear detection of foreground residuals in this case.

A similar  $\chi^2$  test was now performed, but this time to study variation between different number of needlet scales (and thus also different  $\ell_{max}$ ) used for the estimation:

$$\mathbf{d} = \begin{bmatrix} f_{NL}^{31} - f_{NL}^{30} \\ f_{NL}^{30} - f_{NL}^{29} \\ \vdots \\ f_{NL}^{26} - f_{NL}^{25} \end{bmatrix} \quad (13)$$

where the superscript denotes number of needlet scales used to estimate the  $f_{NL}$  value.  $\chi^2$  was found using equation (10) for the WMAP data as well as for the 5000 simulations according to the same procedure as above. This was done for the individual Q, V and W frequency channels, and for the combined V+W map. The test was also performed using a combined data vector from all the three frequency channels. The results (table 4) show that the variation in the  $f_{NL}$  estimate with respect to needlet scales is well within the expected bounds.

## 5. CONCLUSIONS

Freq. channel	% of sim. with higher $\chi^2$
Q	91.9
V	44.3
W	72.2
V + W	76.6
combined Q, V and W	56.3

TABLE 4

TEST OF  $f_{NL}$  VARIATION WITH RESPECT TO SCALE. FRACTION OF SIMULATIONS WITH HIGHER  $\chi^2$  VALUE THAN WMAP DATA. THE RESULTS SHOW THAT THE WMAP DATA IS CONSISTENT WITH GAUSSIANTY IN THIS RESPECT.

We have tested an estimator for  $f_{NL}$  based on the needlet bispectrum (Lan & Marinucci 2008a). We used the estimator to obtain best fit values of  $f_{NL}$  from the WMAP 5 year data, using the combined V+W map as well as the independent frequency channels. The error bars on  $f_{NL}$  obtained with the needlet bispectrum are significantly larger than those obtained by the optimal bispectrum estimator (Smith et al. 2008), but the needlet bispectrum still provides an important and independent test of consistency. We have further introduced a set of consistency tests based on the difference  $\Delta f_{NL} = f_{NL}^1 - f_{NL}^2$  where 1 and 2 refer to different masks, different frequency channels or different number of multipoles. We compare the differences  $\Delta f_{NL}$  for the different cases to the values obtained in simulations.

We find our best estimate of  $f_{NL}$  using the combined bispectrum from the V and W channels giving  $f_{NL} = 76 \pm 38$  using the KQ75 mask and  $\ell_{\max} = 1000$ , consistent within  $1\sigma$  with the value of  $f_{NL} = 51 \pm 32$  obtained by the WMAP team as well as with the values obtained by (Yadav & Wandelt 2008; Smith et al. 2008) all using  $\ell_{\max} = 750$ .

Using the combined V + W map and  $\ell_{\max} = 1000$ , we obtained  $f_{NL} = 84 \pm 40$  for KQ75 and  $f_{NL} = 110 \pm 37$

using KQ85 (corrected for point source bias). This difference in  $f_{NL}$  using the two different masks was found to be within the  $2\sigma$  limit from simulations and thus consistent with expectations. In order to further limit the risk of foreground contamination, we estimated  $f_{NL}$  on an extended KQ75 mask excluding 37% of the sky giving  $f_{NL} = 97 \pm 42$ .

Using the independent frequency channels and the KQ75 cut, we obtained  $f_{NL} = 9 \pm 44$  for the Q band,  $f_{NL} = 105 \pm 42$  for the V band and  $f_{NL} = 54 \pm 45$  for the W band. Such a large difference in  $f_{NL}$  between the bands were found only in 4.5% of the simulations. This is  $2\sigma$  away from the expected value. This could be a sign of foreground residuals but could also well be a statistical fluke. We found the latter explanation to be more reasonable considering that for the smaller KQ85 mask 14% of the simulations had a larger difference. Similar tests were made with values of  $f_{NL}$  obtained using different number of multipoles and channels, and no significant deviations from the expected differences were found. We therefore conclude that there are no convincing evidence of foreground residuals having influenced the estimated value of  $f_{NL}$ , even using the KQ85 galactic cut. However repeating these tests on the next release of the WMAP data and on Planck data will be necessary in order to confirm this claim.

FKH is grateful for an OYI grant from the Research Council of Norway. This research has been partially supported by ASI contract I/016/07/0 "COFIS" and ASI contract Planck LFI Activity of Phase E2. We acknowledge the use of the NOTUR supercomputing facilities. We acknowledge the use of the HEALPix (Górski et al. 2005) package and the Legacy Archive for Microwave Background Data Analysis (LAMBDA). Support for LAMBDA is provided by the NASA Office of Space Science.

## REFERENCES

- Acquaviva, V., Bartolo, N., Matarrese, S. and Riotto, A. 2003, Nucl. Phys. B, 667, 119, arXiv:astro-ph/0209156
- Alishahiha, M., Silverstein, E. and Tong, D. 2004, Phys. Rev. D, 70, 123505
- Arkani-Hamed, N., Creminelli, P., Mukohyama, S. and Zaldarriaga, M. 2004, JCAP, 0404, 001
- Babich, D., Creminelli, P., Zaldarriaga, M. 2004, Journal of Cosmology and Astroparticle Physics 8, 009
- Baldi, P., Kerkycharian, G., Marinucci, D. and Picard, D. 2006, Annals of Statistics, Vol. 37, No. 3, 1150-1171, arxiv:math.st/0606599
- Baldi, P., Kerkycharian, G. Marinucci, D. and Picard, D. 2007, Bernoulli, Vol. 15, n.2, pp. 438-463, arxiv: 0706.4169
- Baldi, P., Kerkycharian, G., Marinucci, D., Picard, D. 2008, Annals of Statistics, in press, arxiv: 0807.5059
- Bartolo, N., Komatsu, E., Matarrese, S. and Riotto, A. 2004a, Phys. Rept., 402, 103
- Bartolo, N., Matarrese, S. and Riotto, A. 2004b, JCAP, 0401, 003
- Bartolo, N., Matarrese, S. and Riotto, A. 2004c, JHEP, 0404, 006
- Buchbinder, E. I., Khoury, J. and Ovrut, B. A. 2008, Phys. Rev. Lett., 100, 171302
- Cabella, P., Hansen, F.K., Liguori, M., Marinucci, D., Matarrese, S., Moscardini, L., and Vittorio, N. 2006, MNRAS, 369, 819
- Creminelli, P. et al. 2006 JCAP, 5, 4
- Cruz, M., Cayon, L., Martinez-Gonzalez, E., Vielva, P. & Jin, J. 2007, ApJ, 655, 11
- Cruz, M., Cayon, L., Martinez-Gonzalez, E., Vielva, P. 2006, MNRAS, 369, 57
- Curto, A. et al 2008, in press, arXiv:0807.0231
- Delabrouille, J., Cardoso, J.-F., Le Jeune, M., Betoule, M., Fay, G. & Guilloux, F. 2008, arxiv 0807.0773
- Dvali, G., Gruzinov, A. and Zaldarriaga, M. 2004, Phys. Rev. D, 69, 023505
- Enqvist, K. and Sloth, M. S. 2002, Nucl. Phys., B626, 395
- Fay, G., Guilloux, F., Betoule, M., Cardoso, J.-F., Delabrouille, J. & Le Jeune, M. 2008a, Phys. Rev. D, D78, 083013
- Fay, G. and Guilloux, F. 2008b, arxiv: 0807.2162
- Geller, D. and Mayeli, A. 2007a, ArXiv.0706.3642
- Geller, D. and Mayeli, A. 2007b, arxiv: 0709.2452
- Geller, D. and Marinucci, D. 2008, arxiv: 0811.2935.
- Geller, D., Hansen, F.K., Marinucci, D., Kerkycharian and Picard, D. 2008, Physical Review D, D78, 123533
- Górski, K.M., E. Hivon, A.J. Banday, B.D. Wandelt, F.K. Hansen, M. Reinecke, and M. Bartelmann, HEALPix: A Framework for High-resolution Discretization and Fast Analysis of Data Distributed on the Sphere, ApJ, 622, 759-771, 2005
- Guilloux, F., Fay, G., Cardoso, J.-F. 2007, arxiv 0706.2598
- Hu, W. 2001, Physical Review D, 64, 8, id.083005
- Kolb, E. W., Riotto, A. and Vallinotto, A. 2005, Phys. Rev. D, 71, 043513
- Kolb, E. W., Riotto, A. and Vallinotto, A. 2006, Phys. Rev. D, 73, 023522
- Komatsu, E. and Spergel, D.N. 2001, Physycal Review D, 63, 063002, arXiv:astro-ph/0005036
- Komatsu, E., Spergel, D. N. & Wandelt, B. D. 2005, ApJ, 634, 14
- Komatsu, E., et al. 2008, ApJS, in press, astro-ph/0803.0547v2
- Koyama, K., Mizuno, S., Vernizzi, F. and Wands, D. 2007, JCAP, 0711, 024

- Lan, X. & Marinucci, D. 2008a, *Electronic Journal of Statistics*, Vol. 2, pp.332-367, (2008), arXiv:0802.4020
- Lan, X., Marinucci, D. 2008b, arxiv: 0805.4154
- Liguori, M. et al. 2007, *Phys. Rev. D*, 76, 105016
- D. Lyth and D. Wands 2002, *Phys. Lett. B*, 524, 5
- Maldacena, J. M. 2003, *JHEP*, 0305, 013 (2003), arXiv:astro-ph/0210603
- Marinucci, D. 2006, *The Annals of Statistics* 34, 1, arxiv:math/0502434
- Marinucci, D., Pietrobon, D., Balbi, A., Baldi, P., Cabella, P., Kerkycharian, G., Natoli, P., Picard, D., Vittorio, N., 2008, *MNRAS*, 383, 539
- Martinez-Gonzalez, E. et al. 2002, *MNRAS*, 336, 22
- Mayeli, A. 2008, arxiv: 0806.3009
- McEwen J.D., Hobson M.P., Lasenby A.N., Mortlock, D.J. 2006, *MNRAS*, 371, L50
- Moroi, T. and Takahashi, T. 2001, *Phys. Lett. B*, 522, 215, [Erratum-ibid. 539, 303 (2002)].
- Narcowich, F.J., Petrushev, P. and Ward, J.D. 2006a, *SIAM Journal of Mathematical Analysis* 38, 2, 574
- Narcowich, F.J., Petrushev, P. and Ward, J.D. 2006b, *Journal of Functional Analysis* 238, 2, 530
- Pietrobon, D., Balbi, A., Marinucci, D. 2006, *Physical Review D*, 74, 043524
- Pietrobon, D. et al. 2008a, arXiv:0812.2478
- Pietrobon, D., Amblard, A., Balbi, A., Cabella, P., Cooray, A. & Marinucci, D. 2008b, *Phys. Rev. D.*, D78, 103504
- Smith, K. M., Senatore, L. & Zaldarriaga, M. 2009, arxiv: 0901.2572
- Vielva P., Martinez-Gonzalez E., Barreiro B., Sanz J. & Cayon L. 2004, *ApJ*, 609, pp. 22
- Yadav, A. S. et al 2007a, arXiv:0711.4933
- Yadav, A. S., Komatsu, E. & Wandelt B. D. 2007b, *ApJ*, 664, 680
- Yadav, A. S. & Wandelt, B. D. 2008, *Phys. Rev. Lett*, 100, 181301
- Yadav, A.P.S., Komatsu, E., Wandelt, B.D. , Liguori, M., Hansen, F.K. and Matarrese, S. 2007, arXiv:0711.4933